## Interplay between numerical relativity and perturbation theory: finite size effects

Tousif Islam<sup>1,2,3,\*</sup> and Gaurav Khanna<sup>4,1,3</sup>

<sup>1</sup>Department of Physics, University of Massachusetts, Dartmouth, MA 02747, USA
<sup>2</sup>Department of Mathematics, University of Massachusetts, Dartmouth, MA 02747, USA
<sup>3</sup>Center for Scientific Computing and Visualization Research, University of Massachusetts, Dartmouth, MA 02747, USA
<sup>4</sup>Department of Physics and Center for Computational Research, University of Rhode Island, Kingston, RI 02881, USA
(Dated: August 9, 2023)

We investigate the interplay between numerical relativity (NR) and point-particle black hole perturbation theory (ppBHPT) in the comparable mass ratio regime. In the ppBHPT framework, the secondary black hole is treated as a point particle, neglecting its finite size. Our study focuses on addressing the missing finite size effect in the ppBHPT framework and proposing a method for incorporating the size of the secondary into the perturbation theory framework. We demonstrate that by considering the secondary as a finite size object, the BHPT waveforms closely match NR waveforms. Additionally, we revisit the  $\alpha$ - $\beta$  scaling technique, which was previously introduced by Islam et al. [1], as a means to effectively match ppBHPT waveforms to NR waveforms. We further analyze the scaling procedure and decompose it into different components, attributing them to various effects, including the corrections arising from the finite size of the secondary black hole.

### I. INTRODUCTION

Efficient detection and accurate characterization of gravitational wave (GW) signals from binary black hole (BBH) mergers require computationally cheap yet accurate multimodal waveform models. The development of such models [2–16] relies heavily on accurate numerical simulations of BBH mergers. The most accurate way to simulate a BBH merger is by solving the Einstein equations using numerical relativity (NR). Significant progress has been made in refining NR pipelines for BBH systems with comparable masses i.e. with  $1 \le q \le 10$  (where  $q := m_1/m_2$ is the mass ratio of the binary with  $m_1$  and  $m_2$  being the mass of the primary and secondary black hole respectively) over the past two decades [17–24]. However, accurately simulating BBH mergers in the intermediate to large mass ratio regime ( $10 \le q \le 100$ ) remains a challenging task. NR simulations in this mass ratio range become computationally demanding due to various factors. As a result, accurately modeling GW signals from BBH mergers in this regime using NR simulations becomes increasingly difficult.

On the other hand, point particle black hole perturbation theory (ppBHPT) [25–34] provides an accurate modeling approach for extreme mass ratio binaries ( $q \to \infty$ ). In ppBHPT, the smaller black hole is treated as a point particle orbiting the larger black hole in a curved spacetime background. Substantial progress has been made in accurately simulating BBH mergers in this regime using the ppBHPT framework. However, as the mass ratio becomes less asymmetric and approaches the comparable to intermediate mass ratio regime, the assumptions of the ppBHPT framework start to break down. Consequently, the ppBHPT framework cannot generate accurate gravitational waveforms in this regime.

Understanding the interplay between NR and ppBHPT framework in the comparable to intermediate mass ratio regime is an active and exciting area of research in the field of gravitational waves. Several studies [35–37] have been conducted to investigate the limitations and accuracy of both approaches in this regime.

Recently, significant advancements have been made in expanding the domain of NR and ppBHPT frameworks. These advancements include the development of the BHPTNRSur1dq1e4 surrogate model [1] and a fully relativistic second-order self-force model [38], as well as the expansion of numerical relativity (NR) techniques to simulate BBH mergers with higher mass ratios [39– 42]. The BHPTNRSur1dq1e4 surrogate model, based on the ppBHPT framework, has demonstrated remarkable accuracy in predicting waveforms for BBH mergers in the comparable to large mass ratio regime. Through a simple but non-trivial calibration process called the  $\alpha$ - $\beta$  scaling, the ppBHPT waveforms are rescaled to achieve excellent agreement with NR data specifically in the comparable mass ratio regime. In parallel, the fully relativistic secondorder self-force model has also shown promising results in accurately reproducing NR waveforms in the comparable mass ratio regime.

In this paper, we investigate the interplay between NR and ppBHPT framework in the comparable mass ratio regime through the lens of the  $\alpha$ - $\beta$  scaling. In particular, we focus on understanding the corrections due to the missing finite size of the secondary black hole in ppBHPT framework and proposing a robust method for incorporating the size of the secondary into the perturbation theory framework. The remaining sections of the paper are structured as follows. Section II provides a concise overview of ppBHPT, the  $\alpha$ - $\beta$  scaling, and the perturbation theory framework that partially incorporates the size of the secondary black hole. In Section III, we present our main findings and results. To begin, Section III A focuses on estimating the expected size of the secondary black hole. Next, in Section III B, we delve into the im-

<sup>\*</sup> tislam@umassd.edu

pact of considering the finite size of the secondary within the BHPT framework on the waveform. Section III C demonstrates the close agreement between the BHPT waveforms, incorporating the finite size secondary, and the NR waveforms. Finally, in Section IV, we revisit the  $\alpha$ - $\beta$  scaling and offer a detailed breakdown of its components. We attribute these components to different effects, including the corrections arising from the finite size of the secondary black hole.

#### II. BLACK HOLE PERTURBATION THEORY

In this section, we present a concise summary of the perturbative techniques employed in this work to generate waveforms from BBH mergers in the comparable mass ratio regime.

### A. Point-particle perturbation theory

In the ppBHPT framework, the smaller black hole is modeled as a point-particle with no internal structure and a mass of  $m_2$ , moving in the spacetime of the larger Kerr black hole with mass  $m_1$  and spin angular momentum per unit mass a. Here, we provide an executive summary of this framework and refer to Refs. [25–28] for additional details. First, we compute the trajectory taken by the point-particle and then we use that trajectory to compute the gravitational wave emission.

During the initial adiabatic inspiral, the particle follows a sequence of geodesic orbits driven by radiative energy and angular momentum losses. The flux radiated to null infinity and through the event horizon are computed by solving the frequency-domain Teukolsky equation[29–32] using the open-source code GremlinEq [33, 34] from the Black Hole Perturbation Toolkit [43]. The inspiral trajectory is then extended to include a plunge geodesic and a smooth transition region following a procedure similar to one proposed by Ori-Thorne [44]. We compute the transition between initial inspiral and the plunge using a generalized Ori-Thorne algorithm [45, 46]. Our trajectory model does not include the effects of the conservative or second-order self-force [47].

Once the trajectory of the perturbing compact body is fully specified, we solve the inhomogeneous Teukolsky equation in the time-domain while feeding the trajectory information into the particle source-term of the equation [25–28, 48]. This involves a four step procedure: (i) rewriting the Teukolsky equation using compactified hyperboloidal coordinates is shown using standard Boyer-Lindquist coordinates that allow us to extract the gravitational waveform directly at null infinity while also solving the issue of unphysical reflections from the artificial boundary of the finite computational domain; (ii) obtaining a set of (2+1) dimensional PDEs by using the axisymmetry of the background Kerr space-time, and separating the dependence on azimuthal coordinate; (iii)

recasting these equations into a first-order, hyperbolic PDE system; and finally (iv) implementing a high-order WENO (3,5) finite-difference scheme with Shu-Osher (3,3) time-stepping [48]. The point-particle source term on the right-hand-side of the Teukolsky equation requires some specialized techniques for a finite-difference numerical implementation [25, 26]. We set the spin of the central black hole to a value slightly away from zero,  $a/m_1 = 10^{-8}$  for technical reasons<sup>1</sup>.

#### B. Scaling between perturbation theory and numerical relativity waveforms

While building a ppBHPT based waveform model for comparable to extreme mass ratio binaries Ref. [1] introduced a simple but non-trivial scaling called the  $\alpha$ - $\beta$  scaling between ppBHPT waveforms and NR. It reads:

$$h_{\mathtt{full},\alpha_{\ell},\beta}^{\ell,m}(t;q) \sim \alpha_{\ell} h_{\mathtt{pp}}^{\ell,m}(t\beta;q) ,$$
 (1)

where  $\alpha_\ell$  and  $\beta$  are determined by minimizing the  $L_2$ -norm between the NR and rescaled ppBHPT waveforms. Note that while  $\alpha_\ell$  modifies the amplitude of the various spherical harmonic modes,  $\beta$  changes the time/frequency evolution of the binary by rescaling the time. After this  $\alpha$ - $\beta$  calibration step, the ppBHPT waveforms exhibit remarkable agreement with NR waveforms. For instance, in the comparable mass ratio regime, the dominant quadrupolar mode of the rescaled waveform agrees to NR with errors smaller than  $\approx 10^{-3}$ .

# C. Perturbation theory with finite size of the secondary black hole

To incorporate the effect of a finite sized object in the context of the point-particle approach summarized above, we simply follow the method presented previously in Ref. [49]. In particular, we consider an extended object as a composition of point-particles arranged in a manner consistent with the shape and size of the object. As seen in Ref. [49] the dominant affect arises from the object's extent in the azimuthal  $\varphi$  direction. In fact, the impact on the wave amplitude of the  $h_{\ell m}$  mode can be computed by introducing an analytical factor as derived in Sec. IV in Ref. [49] for circular orbits of radius  $r_0$ . The factor f(m) is given by

$$|f(m)|^2 = 2(1 - \cos \eta)/\eta^2$$
,  $\eta \equiv 2\pi mL/r_0$ . (2)

Here L represents the size of the extended object in the azimuthal direction and m is the multipole mode. It is clear from the above expression that if the size of

<sup>&</sup>lt;sup>1</sup> For example, to avoid a change in the definition of the coordinates from Kerr to Schwarzschild.

the object is small compared to the orbital radius, the factor has little effect. Therefore, the finite size correction is negligible during most of the slow inspiral phase of the binary evolution. However, this factor may deviate strongly from unity as the waveform peaks, i.e. when the orbital radius is close to the light-ring  $r_0=3M$ .

### III. RESULTS

In this section, we now provide a detailed discussion on how to associate a length scale to the secondary black hole in the BHPT framework and its effect on the waveform. Furthermore, we offer a comparison between the waveform of finite-sized BHPT and NR for various spherical harmonic modes.

### A. Estimating the size of the secondary black hole

The horizon area  $\mathcal{A}$  of a Kerr black hole (BH) with mass m and spin  $\chi$  is given by

$$\mathcal{A} = 8\pi \left(\frac{Gm}{c^2}\right)^2 (1 + \sqrt{1 - \chi^2}). \tag{3}$$

This enables us to associate a length scale with the black hole through its radius,

$$r_{\rm H} = \sqrt{\frac{\mathcal{A}}{4\pi}}.\tag{4}$$

In BBH merger simulations, such as in NR simulations, the total mass of the binary is typically normalized to unity in geometric units. The mass of the secondary BH is then determined as follows:

$$m_2 = \frac{1}{1+q}. (5)$$

Subsequently, we estimate the radius of the secondary BH for various mass ratios

$$r_s = \frac{2}{1+a} \tag{6}$$

and present the results in Fig. 1. It is worth noting that while the secondary BH in the ppBHPT framework accurately accounts for its mass, it is treated as a point particle and lacks a notion of radius. Conversely, NR simulations incorporate the size of the secondary BH.

# B. Understanding the effect of finite size in ppBHPT waveforms

After proposing a notion for the expected radius of the secondary black hole, we now delve deeper into investigating the impact of the secondary's size on the waveform. Specifically, we choose q=5 and generate

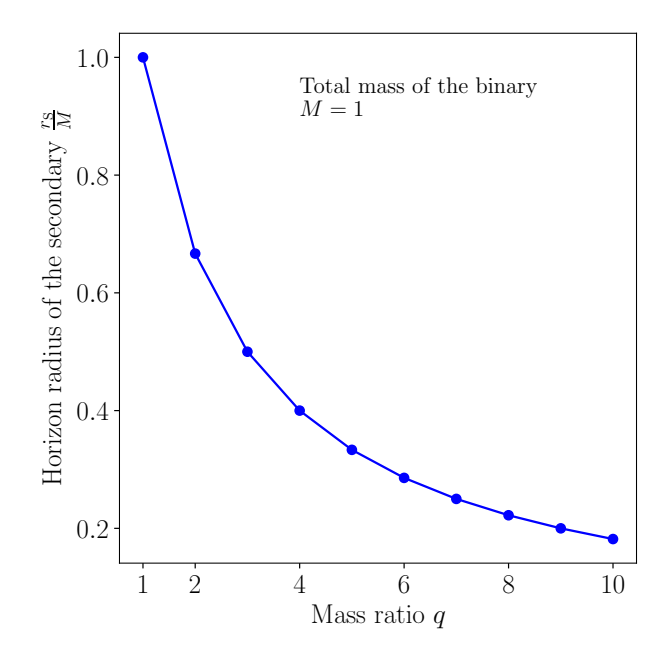


Figure 1. We show the expected horizon radius of the secondary black hole, computed from Eq.(4), as a function of the mass ratio q. More details are in Section III A.

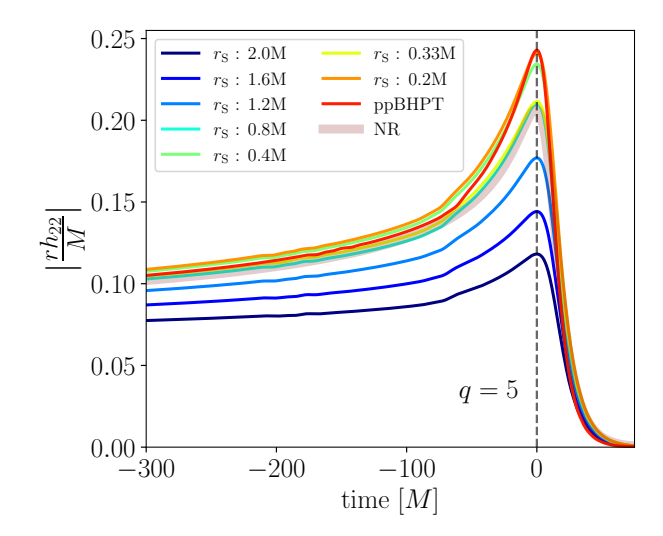


Figure 2. We show the amplitudes of six BHPT waveforms at q=5 generated using a finite size secondary black hole. For comparison, we also include the amplitudes obtained from NR (thick red line) and ppBHPT (thin red line) waveforms. More details are in Section III B.

waveforms using the framework described in Section II C for different sizes of the secondary BH. We simulate BBH mergers for six distinct values of the secondary's radius  $(r_{\rm S}=[0.2,0.4,0.8,1.2,1.6,2.0]M)$ , while keeping the mass of the secondary constant.

In Fig. 2, we present the amplitudes of the BHPT waveforms with varying sizes for the secondary BH. The

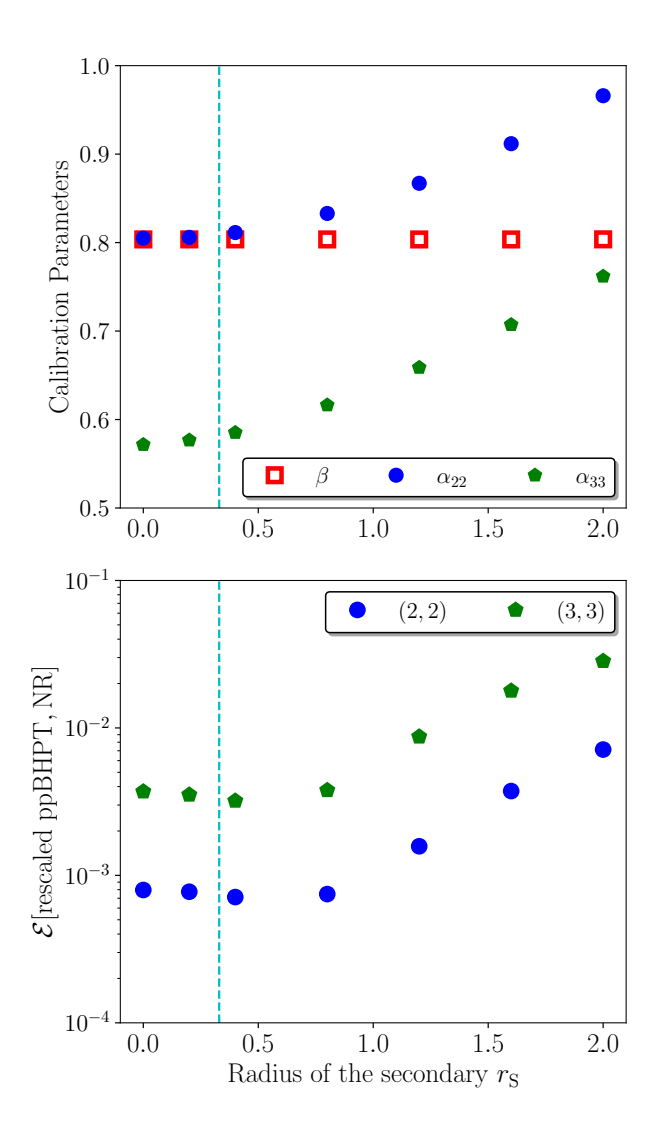


Figure 3. We show the scaling parameters  $\alpha_{22}$ ,  $\alpha_{33}$  and  $\beta$  as a function of the radius of the secondary black hole used in BHPT simulations (upper panel). Furthermore, we show the  $L_2$ -norm error between the rescaled BHPT waveform and NR after the  $\alpha$ - $\beta$  calibration for each simulation (lower panel). Dashed vertical lines denote the expected size of the secondary (i.e.  $r_S = 0.33$ ) from Eq.(4). More details are in Section III B.

waveforms are aligned such that the peak of the (2,2) mode corresponds to t=0M. For comparison, we also include the amplitudes of the ppBHPT and NR waveforms. All the waveforms are scaled with the mass scale of M. To generate the NR waveforms, we utilize the NRHybSur3dq8 waveform model [5], which is a surrogate waveform trained on NR data hybridized with post-Newtonian-corrected effective-one-body inspirals. The use of NRHybSur3dq8 introduces minimal systematic errors in our results, as the error in NRHybSur3dq8 waveforms when compared to NR is close to the error between NR simulations with different resolutions [5]. Specifically, we extract the portion of the NRHybSur3dq8 waveform corresponding to the last

 $\sim 5000M$  of the binary evolution, which corresponds to pure NR waveform data. We observe that the (2, 2) mode amplitude is initially the largest for the ppBHPT waveform. However, as we increase the size of the secondary BH, the amplitude gradually decreases. At a certain point, when the radius of the secondary becomes comparable to or larger than the expected radius for this mass ratio (which is  $r_{\rm S}=0.33M$  as obtained from Eq.(4)), the amplitudes start to exceed those of the NR waveforms.

Next, we proceed with the  $\alpha$ - $\beta$  calibration to the NR waveforms for each of the finite size BHPT waveforms generated. This allows us to determine the calibration parameters  $\alpha_\ell$  and  $\beta$  for the (2,2) and (3,3) modes. We should note that the finite-size BHPT framework, outlined in Section II C, incorporates finite-size effects solely in the fluxes, while retaining the trajectory followed by the point particle. Consequently, these corrections affect only the amplitudes and do not impact the trajectory or the time/frequency evolution. This implies that although we may anticipate different values of  $\alpha_\ell$  for the finite-size BHPT waveforms, the value of  $\beta$  will remain unchanged as compared to the ppBHPT case.

In Fig. 3, we present the scaling parameters as well as the error between the rescaled BHPT and NR data after calibration, plotted as functions of the size of the secondary BH. As expected, the value of the scaling parameter  $\beta$  remains constant regardless of the size of the secondary BH used in waveform generation. Conversely,  $\alpha_{\ell}$  varies as we change the size of the secondary BH. It is also worth noting that as the size of the secondary deviates from the expected value (i.e.  $r_{\rm S}=0.33$ ), the error after calibration begins to increase. This presents an alternative approach to determine the correct size of the secondary by minimizing the error after calibration.

## C. ppBHPT waveforms with correct size of the secondary

It is promising to observe that assigning a finite size to the secondary black hole alters the waveform amplitude and could potentially offer an alternative method for matching BHPT waveforms to NR without performing any calibration. However, this approach relies on accurately determining the correct size of the secondary black hole from the outset. In this section, we explore whether it is feasible to establish such a framework. To begin with, we opt to employ the expected size of the secondary black hole, as estimated from Eq.(4), as the input for our finite size BHPT simulation. It is somewhat encouraging to observe that, in Fig. 3 for q = 5, the error after the  $\alpha$ - $\beta$  calibration exhibits the minima very close to the expected radius obtained from Eq.(4).

We generate finite size BHPT waveforms for four different mass ratios: q=[4,5,8,10]. Subsequently, we compare these waveforms, particularly their amplitudes,

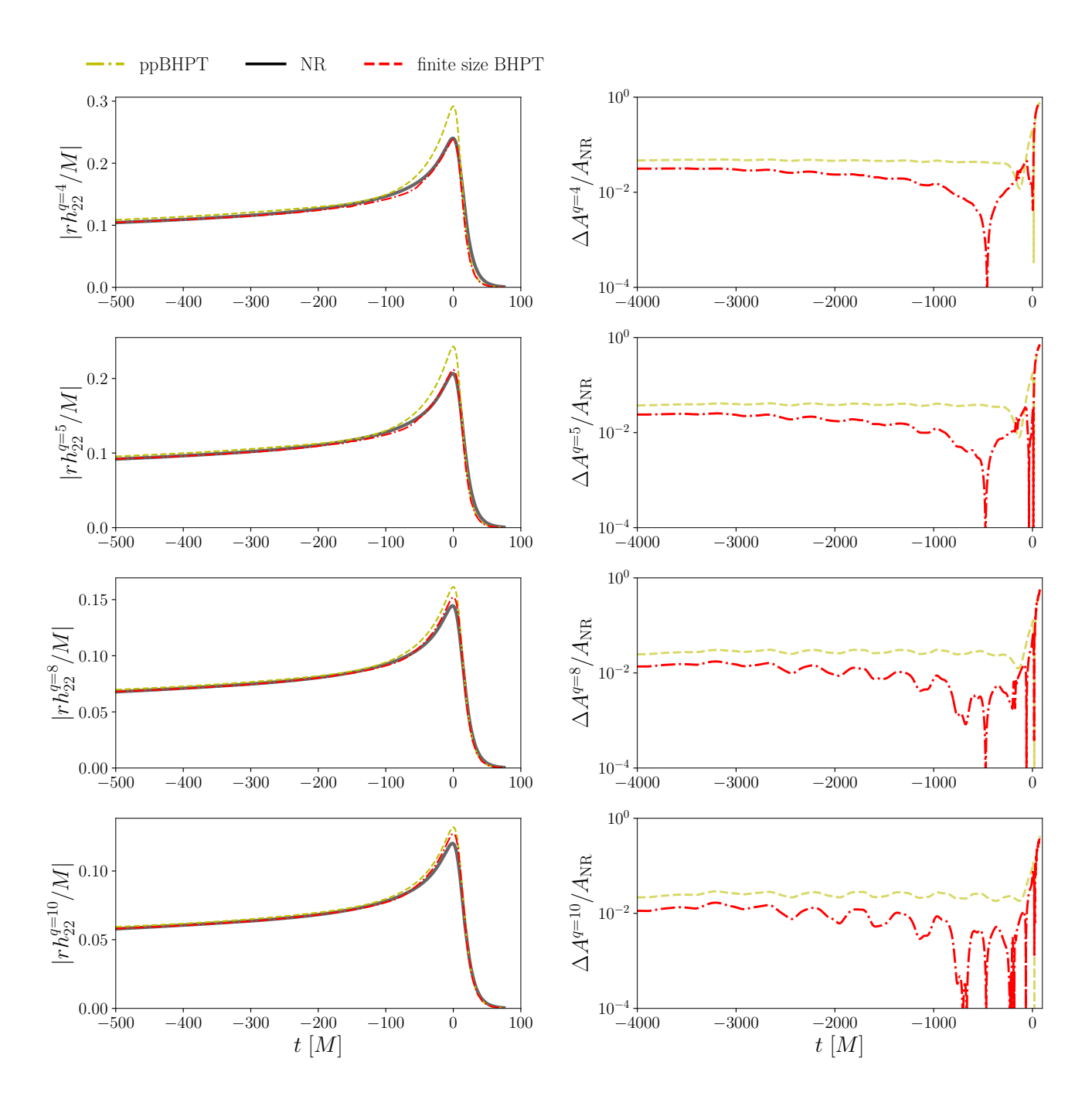


Figure 4. We compare the amplitudes of the  $(\ell, m) = (2, 2)$  mode between finite size BHPT waveforms (red dashed lines), NR (solid black lines), and ppBHPT (yellow dashed lines) for mass ratios q = [4, 5, 8, 10] (left panels). Additionally, we present the corresponding relative errors with respect to NR (right panels). More details are in the text (Sec. III C).

with both NR<sup>2</sup> and ppBHPT waveforms. In Figure 4 (left panels), we present the (2,2) mode amplitudes of the finite size waveforms, as well as those of the NR and ppBHPT waveforms. We observe that while ppBHPT waveforms consistently exhibit larger amplitudes than the

NR data, the finite size BHPT waveforms closely match the amplitudes of NR waveforms for all the mass ratios examined in this study. To gain a deeper understanding of this agreement, we also plot the relative differences in the amplitudes compared to the NR data for both ppBHPT and finite size BHPT waveforms (right panels of Figure 4). Remarkably, we observe that the finite size BHPT waveforms consistently yield errors that are

 $<sup>^2</sup>$  We use NRHybSur3dq8 waveforms as a proxy of the NR data

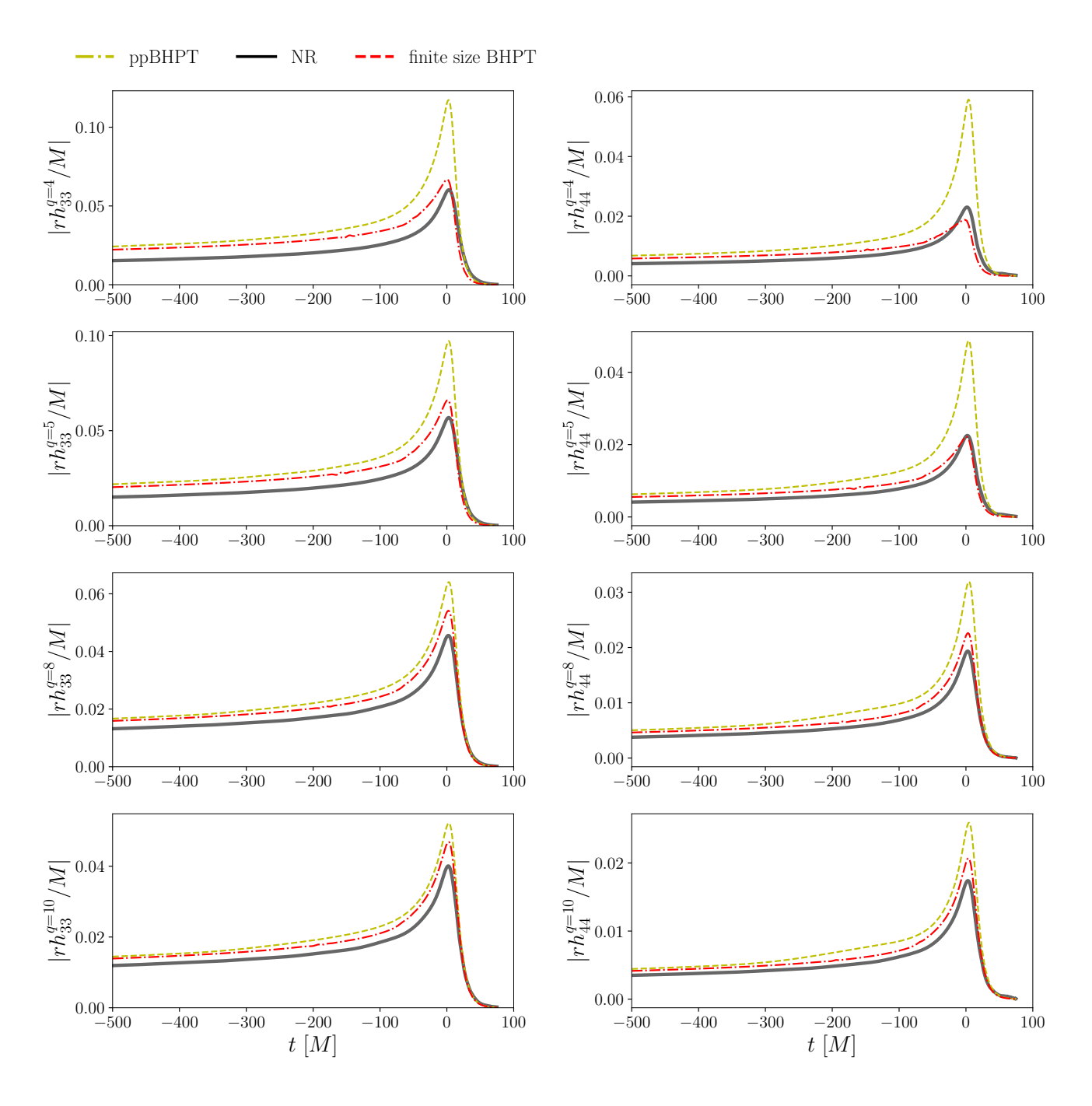


Figure 5. We compare the amplitudes of the  $(\ell, m) = (3, 3)$  and  $(\ell, m) = (4, 4)$  mode between finite size BHPT waveforms (red dashed lines), NR (solid black lines), and ppBHPT (yellow dashed lines) for mass ratios q = [4, 5, 8, 10] (left panels). Additionally, we present the corresponding relative errors with respect to NR (right panels). More details are in the text (Sec. III C).

approximately one order of magnitude smaller than the errors between ppBHPT and NR waveforms. This clearly demonstrates the potential of the finite size BHPT framework in providing accurate waveforms in the regime of comparable mass ratios.

Next, we turn our attention to the higher order modes, specifically the (3,3) and (4,4) modes. We find that even with the inclusion of the expected size of the secondary

in our BHPT simulations, the amplitudes of these higher order modes still exceed those of NR waveforms (Figure 5). It is worth noting that the most significant impact of the finite size secondary is observed around the merger, where the amplitude of the finite size BHPT waveform decreases significantly. As expected, the effects of finite size corrections are more pronounced for smaller mass ratios, such as q=4, compared to larger mass ratios, such

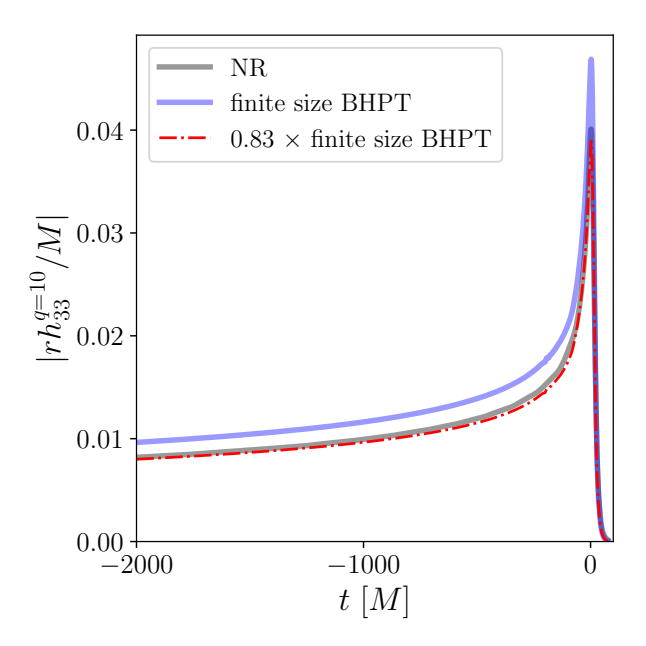


Figure 6. We show the (3,3) mode amplitudes of the NR and finite size BHPT waveforms for q = 10 as well as the scaling between them. More details are in Section III C.

as q = 10.

We further observe that the amplitude ratio between the finite size BHPT waveform and NR waveform follows roughly similar scaling for both the (3,3) and (4,4)modes. Specifically, for a mass ratio of q = 10, we find the following approximate relation:

$$A_{33,NR}^{q=10} \approx 0.81 \times A_{33,fsBHPT}^{q=10},$$
 (7)

$$\begin{split} A_{33,\mathrm{NR}}^{q=10} &\approx 0.81 \times A_{33,\mathrm{fsBHPT}}^{q=10}, \\ A_{44,\mathrm{NR}}^{q=10} &\approx 0.80 \times A_{44,\mathrm{fsBHPT}}^{q=10}, \end{split} \tag{7}$$

where  $A_{33,NR}$  and  $A_{33,fsBHPT}$  represent the (3,3) mode amplitudes of the NR and finite size BHPT waveforms respectively. As an example, in Fig. 6, we show  $A_{33,NR}$ and  $A_{33,\text{fsBHPT}}$  as well as the scaling for q=10. We identify that the numbers 0.83 and 0.81 closely match the transformation factor  $\nu q$  between waveforms expanded in terms of  $\frac{1}{q}$  and  $\nu$ . For q=10, this transformation factor is 0.79. We generalize this relation as:

$$A_{\ell \neq 2.\text{NR}}^q \approx \xi_{\ell \neq 2,q} \times A_{\ell \neq 2.\text{fsBHPT}}^q,$$
 (9)

where  $\xi_{\ell \neq 2,q}$  is the scaling parameter required to match a finite size BHPT mode amplitude to NR. In Figure 7, we present the scaling factors  $\xi_{\ell,q}$  extracted for both the (3,3) and (4,4) modes across the four mass ratio values studied. Interestingly, we find that these scaling factors can largely be attributed to the simple scaling from the  $\frac{1}{a}$  expansion to the  $\nu$  expansion as mentioned earlier.

It is important to note that the finite size effect is smaller for the dominant (2, 2) mode. Consequently, the discrepancies in amplitudes observed in Figure 5 or Figure 6 may not be easily discernible for this mode. Therefore, when comparing waveforms generated with NR and

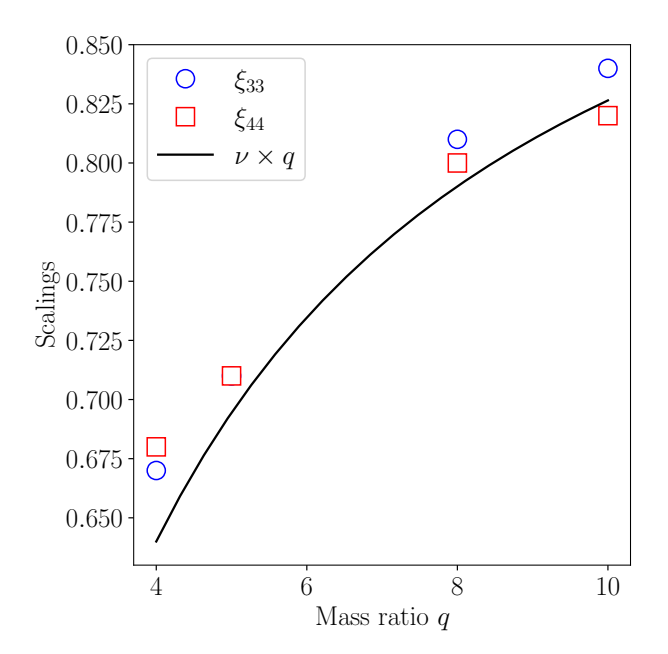


Figure 7. We show the scaling factor  $\xi_{\ell\neq 2,q}$ , required to match a finite size BHPT mode amplitude to NR, as a function of the mass ratio q. For comparison, we also show the expected transformation factor  $(\nu q)$  between expanded in terms of  $\frac{1}{q}$ and  $\nu$ . More details are in Section III C.

BHPT frameworks, it becomes crucial to consider the higher order modes.

### MODELLING THE FINITE SIZE EFFECT

Based on the results presented in Section III C, we now aim to revisit the  $\alpha$ - $\beta$  calibration procedure and break it down into smaller components to identify the effects of finite size.

In Ref. [1], fitting formulae for the calibration parameters  $\alpha_{\ell}$  and  $\beta$  have been developed for the  $\alpha$ - $\beta$  calibration procedure, as a function of the mass ratio q. These formulae read:

$$\alpha_{\ell}(q) = 1 + \frac{A_{\alpha,\ell}}{q} + \frac{B_{\alpha,\ell}}{q^2} + \frac{C_{\alpha,\ell}}{q^3} + \frac{D_{\alpha,\ell}}{q^4},$$
 (10)

and

$$\beta(q) = 1 + \frac{A_{\beta}}{q} + \frac{B_{\beta}}{q^2} + \frac{C_{\beta}}{q^3} + \frac{D_{\beta}}{q^4}.$$
 (11)

Values of the fit coefficients are given in Table I and Table II for  $\alpha_{\ell}$  and  $\beta$ , respectively.

The calibration parameters  $\alpha_{\ell}$  and  $\beta$  account for two distinct effects in the context of the  $\alpha$ - $\beta$  calibration procedure: (i) the difference in mass scales between ppBHPT and NR; and (ii) the absence of finite size effects in the ppBHPT waveforms. Specifically, the mass scale in NR simulations is determined by the total mass of the binary

$\ell$	$A_{\alpha,\ell}$	$B_{lpha,\ell}$	$C_{lpha,\ell}$	$D_{lpha,\ell}$
2	$-1.330\pm0.007$	$2.720{\pm}0.116$	$-5.904 \pm 0.556$	$5.548 \pm 0.833$
3	$-3.067\pm0.017$	$6.244 {\pm} 0.265$	$-9.944 \pm 1.261$	$6.437 \pm 1.894$
4	$-3.909\pm0.032$	$9.431 {\pm} 0.498$	$-14.734\pm2.367$	$9.744 \pm 3.556$
5	$-4.509\pm0.102$	$4.751{\pm}1.554$	$21.959 \pm 7.381$	$-52.350 \pm 11.085$

Table I. Fitting coefficients for  $\alpha_{\ell}$  parameters as defined in Eq.(10).

$A_{eta}$	$B_{eta}$	$C_{eta}$	$D_{eta}$
$-1.238\pm0.003$	$1.596 \pm 0.049$	$-1.776 \pm 0.237$	$1.0577 {\pm} 0.356$

Table II. Fitting coefficients for  $\beta$  parameters as defined in Eq.(11).

M, whereas the mass scale used in ppBHPT corresponds to the mass of the primary black hole  $m_1$ . As a result, the transformation factor between the two mass scales can be expressed as  $\frac{1}{1+1/q}$ . Furthermore, the findings presented in Section III C suggest that even after incorporating the expected size of the secondary, the amplitude of the higher order modes needs to be rescaled by a factor that closely resembles a transformation between the  $\frac{1}{q}$  expansion and the  $\nu$  expansion. Furthermore, we observe that such a correction is unnecessary for the (2,2) mode.

Based on the results presented in Section III C, we can decompose the  $\alpha$ - $\beta$  scaling into individual components and approximately determine the corrections resulting from finite size effects as:

$$\alpha_{\ell=2} = \frac{1}{1 + 1/q} \times \alpha_{\ell,\text{size}} \tag{12}$$

and

$$\alpha_{\ell \neq 2} = \frac{1}{1 + 1/q} \times (\nu q) \times \alpha_{\ell, \text{size}}, \tag{13}$$

where  $\alpha_{\ell,\text{size}}$  represent the finite size corrections in the amplitudes and need to be applied to the ppBHPT waveforms.

It is important to note that although we could not extensively investigate  $\beta$  due to its unchanged nature under the finite size correction implemented in Section II C, it exhibits similar qualitative and quantitative behavior as  $\alpha_{\ell=2}$ . Hence, we express the potential finite-size correction in  $\beta$  as:

$$\beta = \frac{1}{1 + 1/q} \times \beta_{\text{size}},\tag{14}$$

where  $\beta_{\ell,\text{size}}$  is the correction due to the missing finite size of the secondary in ppBHPT framework.

We can establish a connection between the  $\alpha_{\ell}$  and  $\beta$  parameters (obtained from the fits presented in Eq.(10) and Eq.(11)) and the radius of the secondary black hole (obtained from Eq.(4)) for various mass ratios ranging from q=3 to q=8. This in turn gives us the connection between  $\alpha_{\ell,\text{size}}$  ( $\beta_{\ell,\text{size}}$ ) and the radius of the secondary (Fig. 8).

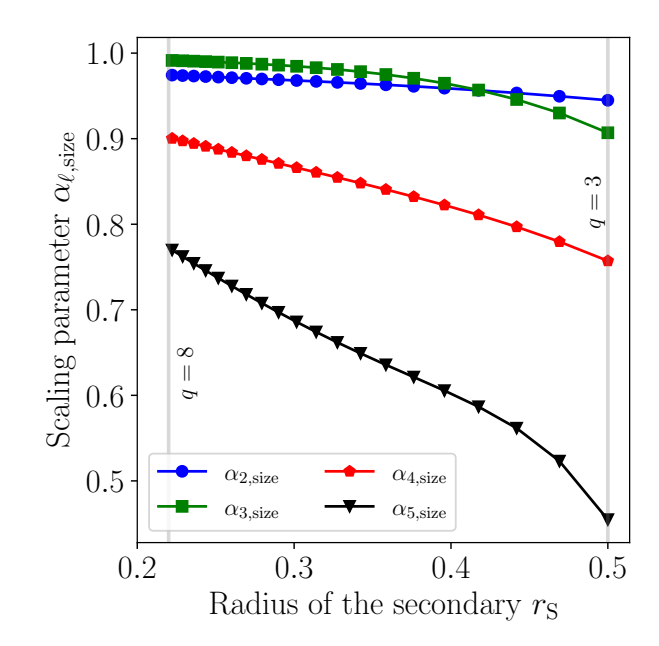


Figure 8. We show the calibration parameters  $\alpha_{\ell, \rm size}$ , which correct for the missing finite size effects, utilized in the  $\alpha$ - $\beta$  scaling of the BHPTNRSur1dq1e4 model, as a function of  $r_{\rm S}$ , the expected radius of the secondary black hole. Vertical grey lines indicate q=3 and q=8. More details are in Section IV.

This connection reveals the following behaviors:

$$\alpha_{\ell=2,\text{size}} \approx 0.9965083 - 0.1436961 \times r_{\text{S}} + 0.2885172 \times r_{\text{S}}^2 - 0.4157566 \times r_{\text{S}}^3, \quad (15)$$

$$\alpha_{\ell=3, \text{size}} \approx 1.0661084 - 0.7671928 \times r_{\text{S}} + 2.78573195 \times r_{\text{S}}^2 - 3.77344743 \times r_{\text{S}}^3, \quad (16)$$

$$\alpha_{\ell=4,\text{size}} \approx 1.04769829 - 0.98742265 \times r_{\text{S}} + 1.98206353 \times r_{\text{S}}^2 - 2.33710155 \times r_{\text{S}}^3, \quad (17)$$

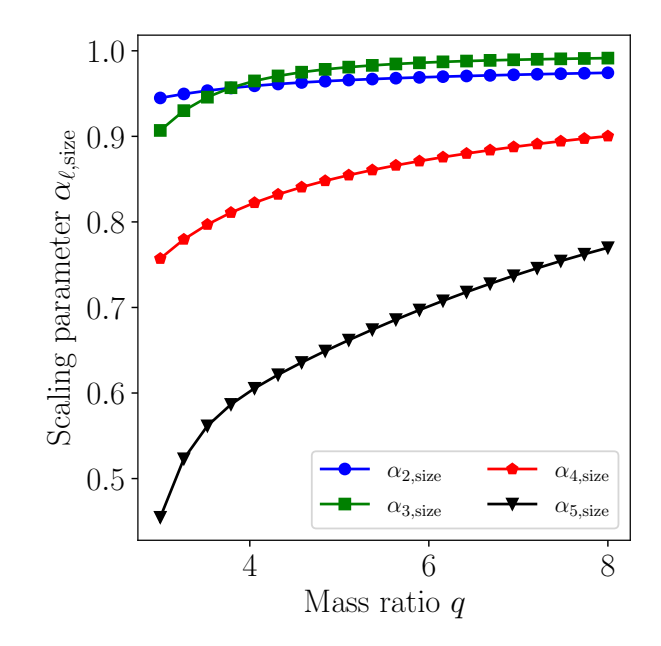


Figure 9. We show the calibration parameters  $\alpha_{\ell, \text{size}}$ , which correct for the missing finite size effects, utilized in the  $\alpha$ - $\beta$  scaling of the BHPTNRSur1dq1e4 model, as a function of the mass ratio q. More details are in Section IV.

$$\alpha_{\ell=5,\text{size}} \approx 1.58061793 - 6.60322364 \times r_{\text{S}} + 17.10135734 \times r_{\text{S}}^2 - 16.75259602 \times r_{\text{S}}^3,$$
(18)

and

$$\beta_{\text{size}} \approx 1.00082016 - 0.1298413 \times r_{\text{S}} + 0.07899518 \times r_{\text{S}}^2 - 0.05206764 \times r_{\text{S}}^3.$$
 (19)

It should be noted that smaller values of  $\alpha_{\ell, \rm size}$  correspond to larger corrections due to finite size effects. As anticipated, we observe that  $\alpha_{\ell, \rm size}$  decreases as the value of q decreases, indicating that the finite size effect becomes more significant as the binary approaches an equal mass system. Additionally, the impact of the finite size effect is more pronounced in higher order modes compared to the dominant (2,2) mode (Fig. 8).

Finally, we repeat the fitting in terms of q and obtain:

$$\alpha_{\ell=2,\text{size}} \approx 0.98999937 - 0.14513987 \times (\frac{1}{q})$$

$$+ 0.22474979 \times (\frac{1}{q})^2 - 0.58826966 \times (\frac{1}{q})^3,$$
(20)

$$\alpha_{\ell=3,\text{size}} \approx 1.01037758 - 0.2900019 \times (\frac{1}{q})$$

$$+ 1.81636983 \times (\frac{1}{q})^2 - 5.63171863 \times (\frac{1}{q})^3,$$
(21)

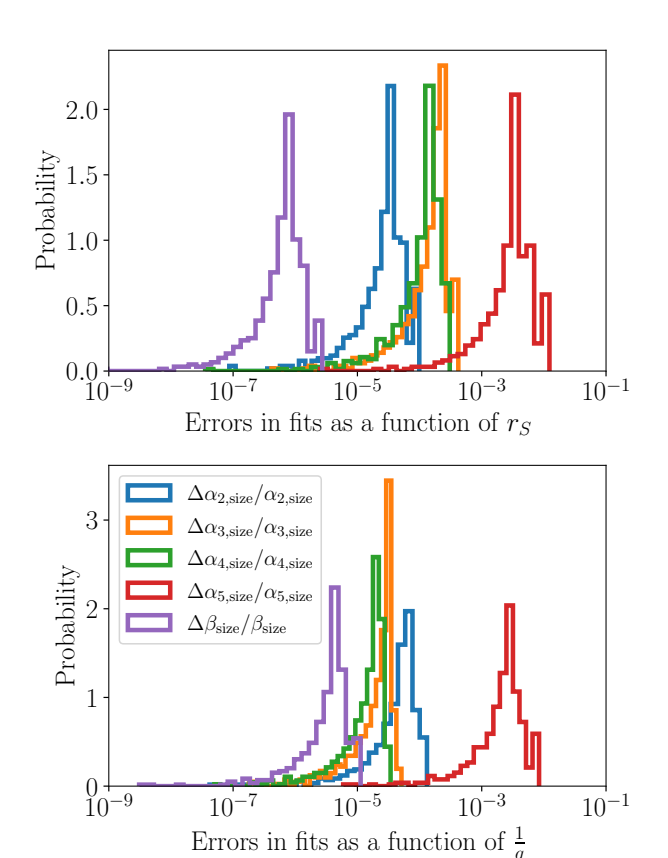


Figure 10. We show the fitting errors in scaling parameters  $\alpha_{\ell,\text{size}}$  and  $\beta_{\text{size}}$  obtained by computing the difference between their numerical values and the values obtained from the analytical fits constructed as a function of both  $r_S$  (upper panel) and  $\frac{1}{a}$  (lower panel). More details are in Section IV.

$$\alpha_{\ell=4,\text{size}} \approx 1.01009073 - 1.1386684 \times (\frac{1}{q})$$

$$+ 2.65047754 \times (\frac{1}{q})^2 - 4.53281099 \times (\frac{1}{q})^3,$$
(22)

$$\alpha_{\ell=5,\text{size}} \approx 1.30116152 - 6.914990 \times (\frac{1}{q})$$
  
  $+ 26.51652 \times (\frac{1}{q})^2 - 40.08021 \times (\frac{1}{q})^3, \quad (23)$ 

and

$$\beta_{\text{size}} \approx 0.9994668 - 0.2303172 \times (\frac{1}{q})$$
  
  $+ 0.3294111 \times (\frac{1}{q})^2 - 0.2743849 \times (\frac{1}{q})^3. \quad (24)$ 

We now compute the fitting errors in the scaling parameters  $\alpha_{\ell,\text{size}}$  and  $\beta_{\text{size}}$  (Fig. 10). To do this, we compare the numerical values of these parameters to the analytical fits constructed in this section. We evaluate the relative

differences for 500 randomly chosen points in the mass ratio range of q=3 to q=8. The fitting errors are found to be very small, with values around  $10^{-6}$  for  $\beta$  regardless of whether the fits are based on  $r_S$  or  $\frac{1}{q}$ . This demonstrates the reliability of the fits.

#### V. DISCUSSION & CONCLUSIONS

In this study, we have investigated the impact of finite size effects on BBH waveform modeling using the BHPT framework (described in Section II C). We explored the behavior of the waveforms by incorporating a finite size for the secondary BH and compared them with both NR and ppBHPT waveforms. One key observation is that the introduction of a finite size for the secondary BH leads to a decrease in waveform amplitudes compared to the ppBHPT waveforms (Section III C; Figs. 4,5).

Additionally, we have performed the  $\alpha$ - $\beta$  calibration (proposed by Islam *et al.* [1]) to match finite size BHPT waveforms with NR waveforms (Section III B; Fig. 2, 3). Interestingly, we found that  $\alpha_{\ell,\text{size}}$  varies as the size of the secondary changes, indicating the specific impact of finite size effects on different multipole modes.

We further extracted the finite size corrections  $\alpha_{\ell, \text{size}}$  and  $\beta_{\text{size}}$  from the calibration parameters  $\alpha_{\ell}$  and  $\beta$  used to rescale a ppBHPT waveform so that it matches NR remarkably well in the comparable mass ratio regime. These corrections provide a systematic way to account for the missing finite size effects in the BHPT framework. We derived fitting formulas for  $\alpha_{\ell, \text{size}}$  and  $\beta_{\text{size}}$  as functions of the mass ratio as well as the expected radius of the secondary, which allows for a convenient determination of these corrections based on the physical properties of the binary system (Section IV; Figs. 8, 9).

Overall, we demonstrated that the amplitude of the finite size BHPT waveforms closely matches that of the NR waveforms for various mass ratios after efficiently incorporating finite size effects in the BHPT framework.

This highlights the potential of accurately modeling BBH waveforms in the comparable mass ratio regime by considering the finite size of the secondary BH. However, further investigations are needed to explore methods for reliably determining the correct size in practical scenarios, as the correct size information is essential for achieving accurate waveform modeling.

It is worth noting that the finite-size BHPT framework (described in Section II C; and in Ref. [49]) solely addresses the absence of finite size effects in the fluxes and amplitudes during the late inspiral-merger-ringdown phase of the waveform. Furthermore, it still relies on the trajectory of the point particle. While these limitations need to be addressed to develop a robust finite-size BHPT framework, it can already provide valuable insights into the dynamics of the binary and the intriguing interplay between NR and BHPT.

Our findings shed light on the interplay between NR and perturbation theory in the context of binary black hole waveforms. They underscore the significance of finite size effects and offer valuable insights into the potential of incorporating them into BHPT waveform models. By bridging the gap between perturbative approaches and NR simulations, these advancements enhance our understanding and modeling capabilities of GW signals from BBH mergers.

#### ACKNOWLEDGMENTS

The authors acknowledge support of NSF Grants PHY-2106755, PHY-2307236 (G.K) and DMS-1912716, DMS-2309609 (T.I and G.K). Simulations were performed on CARNiE at the Center for Scientific Computing and Visualization Research (CSCVR) of UMassD, which is supported by the ONR/DURIP Grant No. N00014181255 and the UMass-URI UNITY supercomputer supported by the Massachusetts Green High Performance Computing Center (MGHPCC).

- [1] Tousif Islam, Scott E. Field, Scott A. Hughes, Gaurav Khanna, Vijay Varma, Matthew Giesler, Mark A. Scheel, Lawrence E. Kidder, and Harald P. Pfeiffer, "Surrogate model for gravitational wave signals from nonspinning, comparable-to large-mass-ratio black hole binaries built on black hole perturbation theory waveforms calibrated to numerical relativity," Phys. Rev. D 106, 104025 (2022), arXiv:2204.01972 [gr-qc].
- [2] Jonathan Blackman, Scott E. Field, Chad R. Galley, Béla Szilágyi, Mark A. Scheel, Manuel Tiglio, and Daniel A. Hemberger, "Fast and Accurate Prediction of Numerical Relativity Waveforms from Binary Black Hole Coalescences Using Surrogate Models," Phys. Rev. Lett. 115, 121102 (2015), arXiv:1502.07758 [gr-qc].
- [3] Jonathan Blackman, Scott E. Field, Mark A. Scheel, Chad R. Galley, Christian D. Ott, Michael Boyle, Lawrence E. Kidder, Harald P. Pfeiffer, and Béla Szilá-

- gyi, "Numerical relativity waveform surrogate model for generically precessing binary black hole mergers," Phys. Rev. **D96**, 024058 (2017), arXiv:1705.07089 [gr-qc].
- [4] Jonathan Blackman, Scott E. Field, Mark A. Scheel, Chad R. Galley, Daniel A. Hemberger, Patricia Schmidt, and Rory Smith, "A Surrogate Model of Gravitational Waveforms from Numerical Relativity Simulations of Precessing Binary Black Hole Mergers," Phys. Rev. D 95, 104023 (2017), arXiv:1701.00550 [gr-qc].
- [5] Vijay Varma, Scott E. Field, Mark A. Scheel, Jonathan Blackman, Lawrence E. Kidder, and Harald P. Pfeiffer, "Surrogate model of hybridized numerical relativity binary black hole waveforms," Phys. Rev. **D99**, 064045 (2019), arXiv:1812.07865 [gr-qc].
- [6] Vijay Varma, Scott E. Field, Mark A. Scheel, Jonathan Blackman, Davide Gerosa, Leo C. Stein, Lawrence E. Kidder, and Harald P. Pfeiffer, "Surrogate models for precess-

- ing binary black hole simulations with unequal masses," Phys. Rev. Research. 1, 033015 (2019), arXiv:1905.09300 [gr-qc].
- [7] Tousif Islam, Vijay Varma, Jackie Lodman, Scott E. Field, Gaurav Khanna, Mark A. Scheel, Harald P. Pfeiffer, Davide Gerosa, and Lawrence E. Kidder, "Eccentric binary black hole surrogate models for the gravitational waveform and remnant properties: comparable mass, nonspinning case," Phys. Rev. D 103, 064022 (2021), arXiv:2101.11798 [gr-qc].
- [8] Alejandro Bohé et al., "Improved effective-one-body model of spinning, nonprecessing binary black holes for the era of gravitational-wave astrophysics with advanced detectors," Phys. Rev. D 95, 044028 (2017), arXiv:1611.03703 [gr-qc].
- [9] Roberto Cotesta, Alessandra Buonanno, Alejandro Bohé, Andrea Taracchini, Ian Hinder, and Serguei Ossokine, "Enriching the Symphony of Gravitational Waves from Binary Black Holes by Tuning Higher Harmonics," Phys. Rev. D 98, 084028 (2018), arXiv:1803.10701 [gr-qc].
- [10] Roberto Cotesta, Sylvain Marsat, and Michael Pürrer, "Frequency domain reduced order model of aligned-spin effective-one-body waveforms with higher-order modes," Phys. Rev. D 101, 124040 (2020), arXiv:2003.12079 [gr-qc].
- [11] Yi Pan, Alessandra Buonanno, Andrea Taracchini, Lawrence E. Kidder, Abdul H. Mroué, Harald P. Pfeiffer, Mark A. Scheel, and Béla Szilágyi, "Inspiral-mergerringdown waveforms of spinning, precessing black-hole binaries in the effective-one-body formalism," Phys. Rev. D 89, 084006 (2014), arXiv:1307.6232 [gr-qc].
- [12] Stanislav Babak, Andrea Taracchini, and Alessandra Buonanno, "Validating the effective-one-body model of spinning, precessing binary black holes against numerical relativity," Phys. Rev. D 95, 024010 (2017), arXiv:1607.05661 [gr-qc].
- [13] Sascha Husa, Sebastian Khan, Mark Hannam, Michael Pürrer, Frank Ohme, Xisco Jiménez Forteza, and Alejandro Bohé, "Frequency-domain gravitational waves from nonprecessing black-hole binaries. I. New numerical waveforms and anatomy of the signal," Phys. Rev. D 93, 044006 (2016), arXiv:1508.07250 [gr-qc].
- [14] Sebastian Khan, Sascha Husa, Mark Hannam, Frank Ohme, Michael Pürrer, Xisco Jiménez Forteza, and Alejandro Bohé, "Frequency-domain gravitational waves from nonprecessing black-hole binaries. II. A phenomenological model for the advanced detector era," Phys. Rev. D 93, 044007 (2016), arXiv:1508.07253 [gr-qc].
- [15] Lionel London, Sebastian Khan, Edward Fauchon-Jones, Cecilio García, Mark Hannam, Sascha Husa, Xisco Jiménez-Forteza, Chinmay Kalaghatgi, Frank Ohme, and Francesco Pannarale, "First higher-multipole model of gravitational waves from spinning and coalescing blackhole binaries," Phys. Rev. Lett. 120, 161102 (2018), arXiv:1708.00404 [gr-qc].
- [16] Sebastian Khan, Katerina Chatziioannou, Mark Hannam, and Frank Ohme, "Phenomenological model for the gravitational-wave signal from precessing binary black holes with two-spin effects," Phys. Rev. D 100, 024059 (2019), arXiv:1809.10113 [gr-qc].
- [17] Abdul H. Mroue et al., "Catalog of 174 Binary Black Hole Simulations for Gravitational Wave Astronomy," Phys. Rev. Lett. 111, 241104 (2013), arXiv:1304.6077 [gr-qc].
- [18] Michael Boyle et al., "The SXS Collaboration catalog of

- binary black hole simulations," Class. Quant. Grav. **36**, 195006 (2019), arXiv:1904.04831 [gr-qc].
- [19] James Healy, Carlos O. Lousto, Yosef Zlochower, and Manuela Campanelli, "The RIT binary black hole simulations catalog," Class. Quant. Grav. 34, 224001 (2017), arXiv:1703.03423 [gr-qc].
- [20] James Healy, Carlos O. Lousto, Jacob Lange, Richard O'Shaughnessy, Yosef Zlochower, and Manuela Campanelli, "Second RIT binary black hole simulations catalog and its application to gravitational waves parameter estimation," Phys. Rev. D 100, 024021 (2019), arXiv:1901.02553 [gr-qc].
- [21] James Healy and Carlos O. Lousto, "Third RIT binary black hole simulations catalog," Phys. Rev. D 102, 104018 (2020), arXiv:2007.07910 [gr-qc].
- [22] James Healy and Carlos O. Lousto, "Fourth RIT binary black hole simulations catalog: Extension to eccentric orbits," Phys. Rev. D 105, 124010 (2022), arXiv:2202.00018 [gr-qc].
- [23] Karan Jani, James Healy, James A. Clark, Lionel London, Pablo Laguna, and Deirdre Shoemaker, "Georgia Tech Catalog of Gravitational Waveforms," Class. Quant. Grav. 33, 204001 (2016), arXiv:1605.03204 [gr-qc].
- [24] Eleanor Hamilton et al., "A catalogue of precessing black-hole-binary numerical-relativity simulations," (2023), arXiv:2303.05419 [gr-qc].
- [25] Pranesh A. Sundararajan, Gaurav Khanna, and Scott A. Hughes, "Towards adiabatic waveforms for inspiral into Kerr black holes. I. A New model of the source for the time domain perturbation equation," Phys. Rev. D 76, 104005 (2007), arXiv:gr-qc/0703028.
- [26] Pranesh A. Sundararajan, Gaurav Khanna, Scott A. Hughes, and Steve Drasco, "Towards adiabatic waveforms for inspiral into Kerr black holes: II. Dynamical sources and generic orbits," Phys. Rev. D 78, 024022 (2008), arXiv:0803.0317 [gr-qc].
- [27] Pranesh A. Sundararajan, Gaurav Khanna, and Scott A. Hughes, "Binary black hole merger gravitational waves and recoil in the large mass ratio limit," Phys. Rev. D 81, 104009 (2010), arXiv:1003.0485 [gr-qc].
- [28] Anil Zenginoglu and Gaurav Khanna, "Null infinity waveforms from extreme-mass-ratio inspirals in Kerr spacetime," Phys. Rev. X 1, 021017 (2011), arXiv:1108.1816 [gr-qc].
- [29] Ryuichi Fujita and Hideyuki Tagoshi, "New numerical methods to evaluate homogeneous solutions of the Teukolsky equation," Prog. Theor. Phys. 112, 415–450 (2004), arXiv:gr-qc/0410018.
- [30] Ryuichi Fujita and Hideyuki Tagoshi, "New Numerical Methods to Evaluate Homogeneous Solutions of the Teukolsky Equation II. Solutions of the Continued Fraction Equation," Prog. Theor. Phys. 113, 1165–1182 (2005), arXiv:0904.3818 [gr-qc].
- [31] Shuhei Mano, Hisao Suzuki, and Eiichi Takasugi, "Analytic solutions of the Teukolsky equation and their low frequency expansions," Prog. Theor. Phys. 95, 1079–1096 (1996), arXiv:gr-qc/9603020.
- [32] William William Thomas Throwe, High precision calculation of generic extreme mass ratio inspirals, Ph.D. thesis, Massachusetts Institute of Technology (2010).
- [33] Stephen O'Sullivan and Scott A. Hughes, "Strong-field tidal distortions of rotating black holes: Formalism and results for circular, equatorial orbits," Phys. Rev. D 90, 124039 (2014), [Erratum: Phys.Rev.D 91, 109901 (2015)],

- arXiv:1407.6983 [gr-qc].
- [34] Steve Drasco and Scott A. Hughes, "Gravitational wave snapshots of generic extreme mass ratio inspirals," Phys. Rev. D 73, 024027 (2006), [Erratum: Phys.Rev.D 88, 109905 (2013), Erratum: Phys.Rev.D 90, 109905 (2014)], arXiv:gr-qc/0509101.
- [35] Carlos O. Lousto, Hiroyuki Nakano, Yosef Zlochower, and Manuela Campanelli, "Intermediate Mass Ratio Black Hole Binaries: Numerical Relativity meets Perturbation Theory," Phys. Rev. Lett. 104, 211101 (2010), arXiv:1001.2316 [gr-qc].
- [36] Carlos O. Lousto, Hiroyuki Nakano, Yosef Zlochower, and Manuela Campanelli, "Intermediate-mass-ratio black hole binaries: Intertwining numerical and perturbative techniques," Phys. Rev. D 82, 104057 (2010), arXiv:1008.4360 [gr-qc].
- [37] Hiroyuki Nakano, Yosef Zlochower, Carlos O. Lousto, and Manuela Campanelli, "Intermediate-mass-ratio black hole binaries II: Modeling Trajectories and Gravitational Waveforms," Phys. Rev. D 84, 124006 (2011), arXiv:1108.4421 [gr-qc].
- [38] Barry Wardell, Adam Pound, Niels Warburton, Jeremy Miller, Leanne Durkan, and Alexandre Le Tiec, "Gravitational waveforms for compact binaries from second-order self-force theory," (2021), arXiv:2112.12265 [gr-qc].
- [39] Carlos O. Lousto and James Healy, "Exploring the Small Mass Ratio Binary Black Hole Merger via Zeno's Dichotomy Approach," Phys. Rev. Lett. 125, 191102 (2020), arXiv:2006.04818 [gr-qc].
- [40] Carlos O. Lousto and James Healy, "Study of the Intermediate Mass Ratio Black Hole Binary Merger up to 1000:1 with Numerical Relativity," (2022), arXiv:2203.08831 [gr-qc].
- [41] Jooheon Yoo, Vijay Varma, Matthew Giesler, Mark A. Scheel, Carl-Johan Haster, Harald P. Pfeiffer, Lawrence E.

- Kidder, and Michael Boyle, "Targeted large mass ratio numerical relativity surrogate waveform model for GW190814," Phys. Rev. D **106**, 044001 (2022), arXiv:2203.10109 [gr-qc].
- [42] Matthew Giesler, Mark A. Scheel, and Saul A. Teukolsky, "Numerical simulations of extreme mass ratio binary black holes," (2022), in preparation.
- [43] "Black Hole Perturbation Toolkit," (bhptoolkit.org).
- [44] Amos Ori and Kip S. Thorne, "The Transition from inspiral to plunge for a compact body in a circular equatorial orbit around a massive, spinning black hole," Phys. Rev. D 62, 124022 (2000), arXiv:gr-qc/0003032.
- [45] Scott A. Hughes, Anuj Apte, Gaurav Khanna, and Halston Lim, "Learning about black hole binaries from their ringdown spectra," Phys. Rev. Lett. 123, 161101 (2019), arXiv:1901.05900 [gr-qc].
- [46] Anuj Apte and Scott A. Hughes, "Exciting black hole modes via misaligned coalescences: I. Inspiral, transition, and plunge trajectories using a generalized Ori-Thorne procedure," Phys. Rev. D 100, 084031 (2019), arXiv:1901.05901 [gr-qc].
- [47] Tanja Hinderer and Eanna E. Flanagan, "Two timescale analysis of extreme mass ratio inspirals in Kerr. I. Orbital Motion," Phys. Rev. D 78, 064028 (2008), arXiv:0805.3337 [gr-qc].
- [48] S. E. Field, S. Gottlieb, Z. J. Grant, L. F. Isherwood, and G. Khanna, "A GPU-Accelerated Mixed-Precision WENO Method for Extremal Black Hole and Gravitational Wave Physics Computations," Commun. Appl. Math. Comput. (2021), 10.1007/s42967-021-00129-2, arXiv:2010.04760 [math.NA].
- [49] Enrico Barausse, Emanuele Berti, Vitor Cardoso, Scott A. Hughes, and Gaurav Khanna, "Divergences in gravitational-wave emission and absorption from extreme mass ratio binaries," Phys. Rev. D 104, 064031 (2021).